

The Eurasia Proceedings of Science, Technology, Engineering & Mathematics (EPSTEM), 2023

Volume 26, Pages 770-779

IConTES 2023: International Conference on Technology, Engineering and Science

Metal Artifact Reduction in CT Images through Sinogram Data Inpainting

Abdessalem Benammar

Research Center in Industrial Technologies (CRTI)

Aicha Allag

Research Center in Industrial Technologies (CRTI)

Imad Araar

Research Center in Industrial Technologies (CRTI)

Ahmed Benyahia

Research Center in Industrial Technologies (CRTI)

Redouane Draï

Research Center in Industrial Technologies (CRTI)

Abstract: When metallic implants are present within the human body, they frequently introduce metallic artifacts into X-ray CT images. These artifacts can lead to significant distortions, obscuring critical information and potentially degrading the quality of the CT images, thereby impacting diagnostic accuracy for clinicians. In recent years, there has been extensive research aimed at mitigating the challenges posed by metallic artifacts, resulting in the development of multiple solutions to address this issue. In this study, we present an efficient approach for artifact removal. Our method involves utilizing the image reconstructed from a sinogram affected by artifacts to generate a synthesized sinogram, deviating from the conventional acquisition of sinogram data. The key stages of our approach encompass segmentation, sinogram gap-filling, and subsequent image enhancement. To achieve rapid segmentation, we employed a K-means classification method. For the retrieval of missing data, we utilized an interpolation algorithm based on a penalized least squares method. In the final phase of image reconstruction enhancement, we implemented an advanced contrast equalization technique to restore image intensities to their inherent dynamic range. Through rigorous verification using both simulated and clinical data, our method consistently demonstrates a remarkable improvement in image quality.

Keywords: Computed tomography, Image reconstruction, Metal artifact, Segmentation, Inpainting sinogram, Contrast enhancement.

Introduction

Implanted medical devices like dental fillings and orthopedic implants can give rise to artifacts in computed tomography (CT) images. These artifacts are introduced through processes such as scattering, partial volume effects, aliasing, beam hardening, and photon starvation (Bamberg et al., 2011; King et al., 2022). In the field of medicine, the increasing use of high-density metallic inserts within the human body, such as dental implants, surgical clips, and steel hip or shoulder prostheses, has led to the occurrence of metallic artifacts in tomographic image scans and reconstructions. This phenomenon presents a significant challenge, making it challenging to conduct accurate analyses of specific anatomical regions within the human body (Usman et al., 2020).

- This is an Open Access article distributed under the terms of the Creative Commons Attribution-Noncommercial 4.0 Unported License, permitting all non-commercial use, distribution, and reproduction in any medium, provided the original work is properly cited.

- Selection and peer-review under responsibility of the Organizing Committee of the Conference

© 2023 Published by ISRES Publishing: www.isres.org

Mainly, we can categorize artifacts into the following three forms (Frederique, 2017): a) Streak artifacts, recognizable by the presence of excessive lines in the image. These artifacts stem from errors in mitigation processes resulting from abrupt transitions between two projections or equipment malfunctions. b) Shadow artifacts, marked by a reduction in image intensity. They tend to manifest near high-contrast objects and occur due to deviations in detector responses from expected attenuation values. c) Ring artifacts, characterized by the emergence of ring-shaped patterns within the image. These artifacts arise from errors in one or more detectors, typically due to defects in the detectors themselves or mechanical issues. Typically, the quality of images reconstructed using the conventional filtered back projection algorithm is sufficient for medical diagnosis under normal conditions. However, in specific instances, such as the presence of metal-induced artifacts, the integrity of the scanner signal can be compromised, rendering the assumptions underlying this method inapplicable. Consequently, the resultant image may exhibit pronounced artifacts and provide inaccurate CT data. To address these challenges and minimize such artifacts, various correction methods have been developed over the past two decades. Nevertheless, it's worth noting that this issue remains unresolved to date (Müller et al., 2009). Metal artifact reduction algorithms can typically be categorized into four primary groups: correction of physical effects, interpolation within the projection field, iterative reconstruction, and methods grounded in deep learning techniques (Zhang et al., 2018). In the first group, referred to as direct artifact reduction methods, physical effects are corrected directly. These methods aim to mitigate artifacts caused by phenomena like beam hardening, which occurs in polychromatic X-ray computed tomography when metal is present, without compromising the integrity of the anatomical images. However, in cases involving metals with a high atomic number, the errors can be substantial enough that the aforementioned corrections may not yield satisfactory results (Park et al., 2016). The second group focuses on projections that pass through metallic objects. In these methods, it is assumed that portions of the projections passing through metal objects are missing and are replaced by substitutes, essentially treating metallic objects as completely opaque (Zhang et al., 2011), Mehranian et al., 2013). One commonly used technique in this group is linear interpolation (LI), where the missing data are estimated through linear interpolation from neighboring unaffected projections for each projection view. The third group of methods allows for the iterative reconstruction of images based on weighted or corrected projections (Chang et al., 2019). The fourth group involves metal artifact reduction (MAR) methods that rely on deep learning. These methods apply corrections for metal-induced beam hardening either in the projection domain or in the image domain (Arabi et al., 2021). However, it's important to note that the creation of a successful deep learning model requires a substantial amount of annotated data. Training a deep learning neural network with insufficient data can lead to inaccurate results. Consequently, this process demands significant time and computing power for effective training.

However, given the inherent complexity associated with diverse metal materials, varying sizes, and positions of metallic objects, achieving consistently satisfactory results using a single artifact reduction strategy can be challenging. Therefore, our approach introduces a novel, rapid, and effective method for the removal of metallic artifacts, including streak and shadow artifacts. Our primary contributions lie in the areas of segmentation, gap filling techniques, and image enhancement. In our methodology, we employ a swift segmentation technique based on K-means classification, which takes into account the global characteristics of the entire image. To recover lost data, we utilized an interpolation algorithm based on a penalized least squares method. This technique enables robust smoothing of equidistant data in one dimension and beyond. Furthermore, for enhancing the reconstructed image, we utilize an improved contrast equalization method designed to restore image intensities to their natural dynamic range.

In summary, this article is structured as follows: Section 2 provides an in-depth exploration of the proposed methodology, encompassing segmentation, sinogram inpainting, and the enhancement of the reconstructed image. Section 3 delves into the results achieved through experimentation, encompassing both synthetic and real-world images. Finally, in Section 4, we present our concluding remarks.

Methods

Image Segmentation

The conventional K-means algorithm typically initiates by selecting cluster centers randomly or following specific protocols. Each cluster center serves as a representative for the cluster it encompasses. The K-means method proceeds through iterative steps. In the initial iteration, every data point within the dataset is assigned to a cluster based on its proximity to the cluster centers. Subsequently, in each subsequent iteration, the cluster centers are recalculated, taking into consideration the average values of the features (or values if the feature is a vector) belonging to the cluster elements. Following the recalculation of cluster centers, the memberships for

each data point are updated in accordance with the values of the new cluster centers. If there is no further alteration in the cluster centers, the algorithm concludes its execution.

Let $I_{gray}=\{p_{1G},p_{2G},\dots,p_{nG}\}$ be the set of the gray level values of the pixels of the input image I , so that p_{iG} is the gray level value of the pixel p_i , where $i = 1, 2 \dots, n$, and $C_G=\{c_{1G},c_{2G},\dots,c_{kG}\}$ the centers of the clusters in the grayscale space where the specified number of clusters is k . The value of the distance (p_{iG}, C_G) between the gray value of the pixel i^{th} and the cluster center j^{th} is calculated by equation (1).

$$d(p_i^G, c_i^G) = |p_i^G - c_i^G| \quad (1)$$

An ordinary image comprises a multitude of individual pixels. In accordance with the classical K-means approach, calculating the distance between each pixel and every clustering center during each iteration can be highly time-consuming. A more efficient method involves the utilization of the grayscale image's histogram. The grayscale histogram of a digital image is divided into a set of bins, each representing an integer grayscale value ranging from 0 to 255. Within the histogram, each bin corresponds to a specific integer value, indicating the count of pixels with the same grayscale value (Amorim et al., 2016; Lin et al., 2014). The rapid K-means algorithm, which relies on the grayscale histogram, ensures a significant acceleration of the process. With this approach, the algorithm computes distance values to the cluster centers 256 times, as opposed to n times, for each iteration. A comprehensive breakdown of the steps is provided below:

1.Let's consider the presence of K clusters, with each cluster containing n central vectors

$$c_k = (c_{k,1}, c_{k,2}, \dots, c_{k,n}) \quad (2)$$

With $k = 1, 2, \dots, K$.

2.Calculate the Euclidean distance of each level value to the center of cluster c_k and assign each cluster level value to its nearest center. For example, the Euclidean distance between the value of level r and the cluster center c_k of the k^{th} cluster vector is:

$$d(r, c_k) = \sqrt{(r_1 - c_{k,1})^2 + (r_2 - c_{k,2})^2 + \dots + (r_n - c_{k,n})^2} \quad (3)$$

Where $k = 1, 2, \dots, K$. The r value of the gray level scale is assigned to the cluster c_k from its nearest center.

3. Calculate the mean value of the levels of each cluster and take it as the new center for each cluster.
4. If the new cluster center is similar to the original one, stop the loop; otherwise, repeat steps 1 to 3.

Sinogram Inpainting

The fast K-means algorithm's output yields segmented images of metallic objects. Subsequently, we project the segmented image of the metallic artifact into the sinogram domain. Then, we subtract the original sinogram, constructed from the unaltered image containing the metallic objects, from the sinogram of the metallic artifact. This subtraction process effectively removes the corrupted projection data. To restore the missing projection data, we employ a gap-filling technique. Our proposed sinogram inpainting technique is an automated smoothing method grounded in penalized least squares regression, specifically based on the discrete cosine transform (DCT-PLS). This technique is utilized for predicting missing values within the sinogram. In this context, we adapt it to fill the gaps, seeking the most suitable sinogram for the restoration of the missing projection data (Wang et al., 2012; Garcia et al., 2010). In a recent study, the author (Bamberg et al., 2011) demonstrated that least squares regression (PLS) can be effectively formulated using DCT, which represents data as a sum of cosine functions oscillating at various frequencies. We provide a brief overview of the DCT-PLS algorithm here, with detailed information available in reference. Consider X as a spatiotemporal dataset containing gaps (missing values), and W as a binary array of identical dimensions indicating the presence or absence of missing values. The DCT-PLS algorithm seeks an \hat{X} that minimizes the following expression:

$$F(\hat{X}) = \|W^{1/2}(\hat{X} - X)\|^2 + s\|\nabla^2 \hat{X}\|^2 \quad (4)$$

Where $\|\cdot\|$ is the Euclidean norm, ∇^2 represents the Laplace operator. s is a positive scalar which controls the degree of smoothing: the more s increases, the more the smoothing of \hat{X} increases, W is the diagonal matrix (W_i) which contains the weights $W_i \in [0, 1]$ corresponding to the data X_i . Note that in the presence of missing values, W is simply defined by $W_i = 0$ if X_i is missing, while an arbitrary finite value is assigned to X_i . In this case, the algorithm performs both smoothing and interpolation. Unlike conventional methods which generally work with local linear or cubic interpolations, missing data is assigned to values that are estimated using the data set (Wang et al., 2012). The \hat{X} can be easily achieved by rewriting equation (5) in the form.

$$\hat{P} = RF \times IDCTN \left[\Gamma \times DCTN \left(W \left((P - \hat{P}) + \hat{P} \right) \right) \right] + (1 - RF)\hat{P} \tag{5}$$

$$\Gamma = \frac{1}{1 + \lambda \times s_i}$$

Where DCT and IDCT denote the discrete cosine transform and the inverse discrete cosine transform, respectively, RF is a relaxation factor.

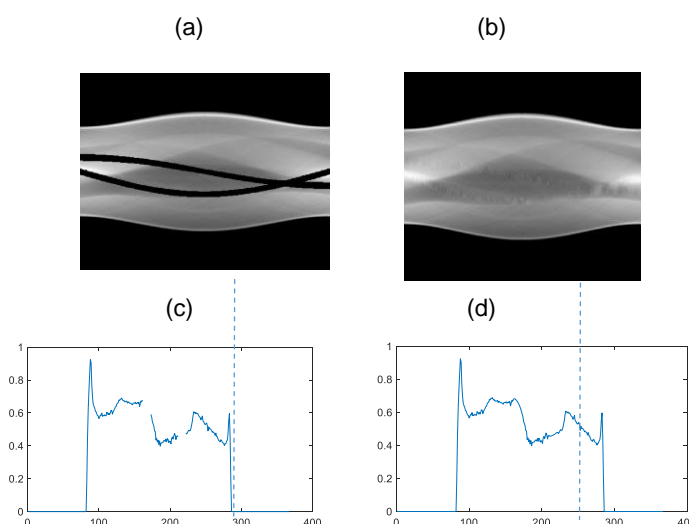


Figure 1. (a) Image of sinogram with removed corrupted projection (metallic objects) from the original sinogram, (b) Inpainted sinogram, The blue dotted lines in the sinogram images represent the central profiles at the 50th view, (c) corrupted projection at the 50th view, (d) corrected projection.

Enhancement of Reconstructed Images

Images generated by various CT scanners often suffer from reduced contrast effects due to inherent limitations. The contrast equalization technique was originally developed as an integral processing step for a novel face recognition system by (Tan et al., 2010). A refined version of this technique has been introduced to enhance SEM images (scanning electron microscopy) for the purpose of achieving visually appealing results (Al-Ameen, 2018). This modification was carried out through empirical experimentation to afford greater control over the enhancement procedure.

With the use of a single parameter, denoted as μ , the outcome of the two-step regularization process is adjusted in a specific manner. Subsequently, when the subsequent two-step mapping process is applied, it fine-tunes the output to generate results characterized by desirable brightness and contrast. Consequently, the μ parameter plays a crucial role in fine-tuning perceived brightness and contrast, subject to the following conditions: ($\mu > 0$), where a higher μ value contributes to enhanced contrast and brightness regularization, whereas a lower μ value results in outcomes with less-than-ideal brightness and contrast. To achieve optimal results, an operator should manually adjust the μ value, starting with a specific value and gradually increasing it until satisfactory results are attained. This process is operator-dependent. The modified two-step regularization process is computed using equations (6) and (7), as outlined below:

$$K(x, y) = \frac{I(x, y)}{(\text{mean}(|I(x', y')|^\mu))^{1/\mu}} \quad (6)$$

where, $I(x, y)$ is the input degraded image; x and y are spatial coordinates; $I(x', y')$ is the transposed version of the image $I(x, y)$; $K(x, y)$ is the image resulting from the first regularization step:

$$L(x, y) = \frac{K(x, y)}{(\text{mean}(\min(\mu, |K(x', y')|)^\mu))^{1/\mu}} \quad (7)$$

$K(x', y')$ is the transposed version of the image $K(x, y)$; $L(x, y)$ is the image resulting from the second regularization step. To further improve the contrast of the regularized image re-map the image intensities in a non-linear and linear fashion, The first step is to use a modified standard logistic function (MSLF), which is a non-linear function for improving contrast. The Conventional Standard Logistics Function (CSLF) is determined using Equation (8):

$$G(x, y) = \frac{\exp(L(x, y))}{1 + \exp(L(x, y))} \quad (8)$$

Where, $G(x, y)$ is the resulting image of the CSLF. In this study, an MSLF is used to allow a better control of the apparent brightness and contrast. The modification is carried out to raise the CSLF to the power of μ as in equation (9).

$$\hat{G}(x, y) = \left(\frac{\exp(L(x, y))}{1 + \exp(L(x, y))} \right)^\mu \quad (9)$$

Where, $\hat{G}(x, y)$ is the resulting image of the MSLF. The output of the above function is an image with altered contrast and attenuated extreme values. To get the final image, the output of equation (9) is normalized to reassign the image intensities to the full dynamic range, which is the second processing step in the proposed new two-step mapping process. This can be done using equation (10).

$$N(x, y) = \frac{\hat{G}(x, y) - \min(\hat{G}(x, y))}{\max(\hat{G}(x, y)) - \min(\hat{G}(x, y))} \quad (10)$$

Where, $N(x, y)$ is the final image resulting from the proposed technique. The proposed technique comprises two primary phases: The first phase involves a two-step regularization process aimed at standardizing the intensities within the input image. The second phase incorporates a two-step mapping process, designed to enhance contrast and restore the image intensities to their original dynamic range. Figures 2b and 2c visually depict the outcomes of the tomographic image enhancement technique in relation to the parameter μ . Notably, the image quality exhibited significant improvement when the value of μ was set to 2.5 (Figure 2c).

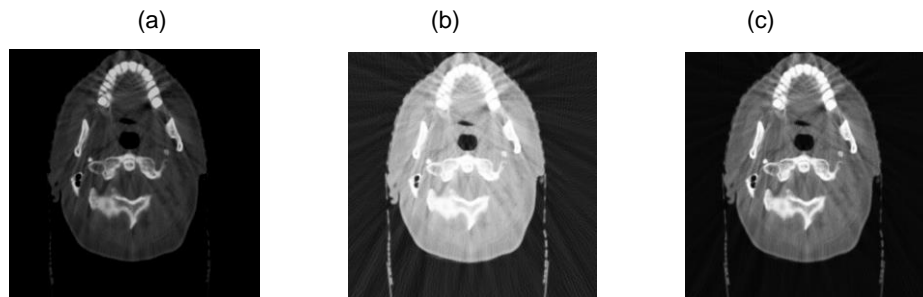


Figure 2. Results obtained by the proposed image enhancement technique, (a) Input image, (b) Enhanced image with $\mu = 1$, (c) Enhanced image with $\mu = 2.5$.

The Proposed Method

The proposed metal artifact reduction algorithm is structured around four fundamental steps:

Step 1: Image Segmentation In the initial step, the input image undergoes segmentation to extract metallic objects. This is achieved through a rapid algorithm grounded in K-means classification, resulting in the isolation of the metallic region within the image.

Step 2: Sinogram Gap Filling In this phase, the metallic area within the image is transformed into the sinogram domain, leading to the acquisition of a metallic trace within the sinogram. Subsequently, by identifying the metallic trace, the corrupted projection data originating from metallic objects is removed from the original sinogram. Finally, a restoration method based on the discrete cosine transform (DCT) is employed to recover the values within the deleted areas.

Step 3: Image Reconstruction and Metallic Object Integration This step involves the reconstruction of the image using the conventional filtered backprojection (FBP) method. Simultaneously, it includes the reintegration of the metallic objects into the reconstructed image.

Step 4: Image Enhancement Through Contrast Equalization The final step focuses on enhancing the reconstructed image by employing a contrast equalization technique. This process is aimed at restoring image intensities to their natural dynamic range.

The overall structure of the proposed algorithm is visually depicted in Figure 3, with each step elaborated in further detail below.

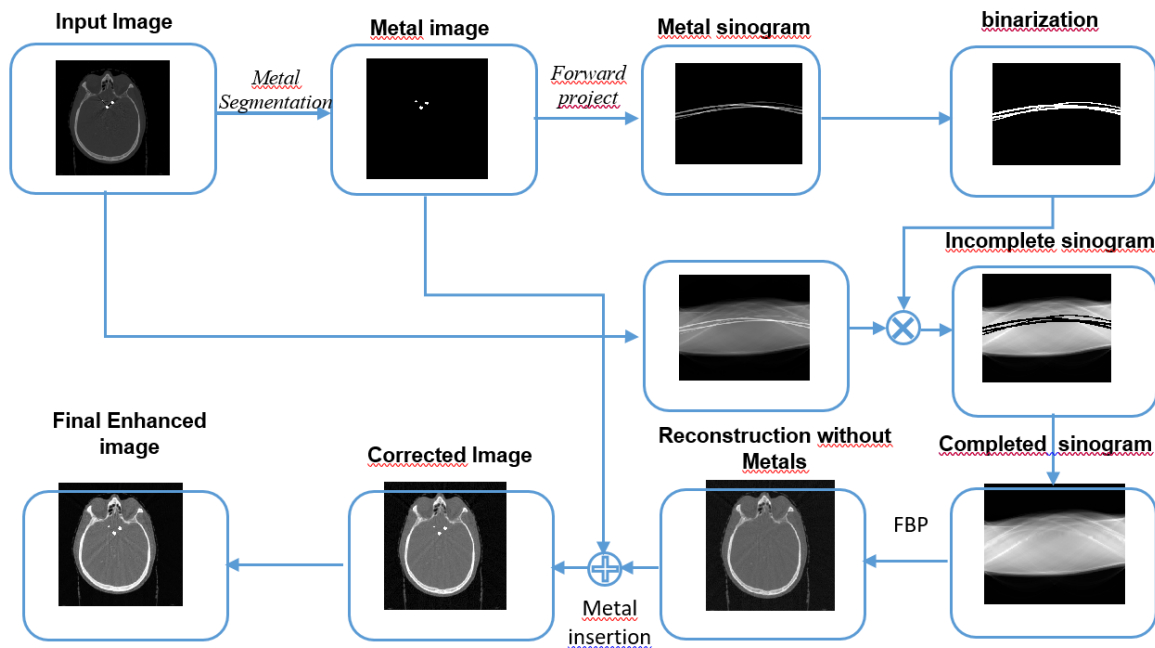


Figure 3. Flowchart of the proposed method

Results and Discussion

To validate the proposed computational approach, a series of experiments were conducted, encompassing both simulated phantom data (utilizing the Shepp-Logan model) and real clinical computed tomography (CT) scans. These tests incorporated images of various dimensions, ranging from 256×256 to 512×512 pixels. The effectiveness of the newly devised Metal Artifact Reduction (MAR) algorithm was assessed using synthetic images containing metallic implants generated through the Iradon method. The acquisition conditions closely mirrored those found in actual CT scans, aligning with the parallel beam geometry characteristic of simulated CT imagery. In the reconstruction phase of the experiments, the Filtered Back Projection (FBP) technique was employed, incorporating the Shepp-Logan filter to suppress high-frequency components. The algorithm's performance was evaluated across a spectrum of progressively intricate phantoms, with Figure 4a illustrating a 256×256 phantom featuring two small artifacts. Figure 4b presents the outcome of the proposed method without any enhancement, while Figure 4c showcases the results achieved with image enhancement techniques applied.

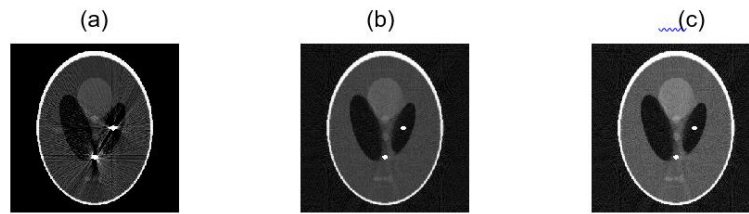


Figure 4. (a) Simulation of a shepp-logan phantom with four metallic artefacts, (b) Result using the proposed correction method, (c) Result of image enhancement technique ($\mu = 2.5$)

Figure 5 depicts the outcomes of our proposed algorithm, with Figure 5(a) showcasing the original phantom containing two substantial metal regions, while Figure 5(b) exhibits the phantom's appearance after being affected by metallic artifacts during the image acquisition process. In our observations, we identified two distinct types of artifacts: hypo-signal and hyper-signal. The results of our algorithmic correction are vividly presented in Figures 5(c) and 5(d). When dealing with multiple metallic regions, the challenge lies in addressing considerably larger gaps in the image, as opposed to the scenario involving a single metallic region. Consequently, a significant amount of information is lost rather than being interpolated. It's worth noting that our proposed algorithm effectively mitigated artifacts in both hypo-signal and hyper-signal areas, as demonstrated in Figure 6.

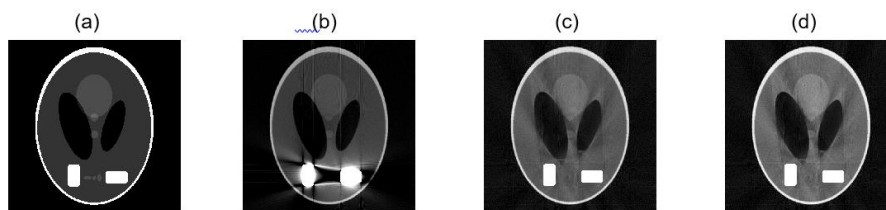


Figure 5. (a) Original Shepp-Logan phantom with two rectangular metallic objects (iron), (b) the original phantom with the influence of metallic artifacts in the acquisition, Results of the proposed algorithm: (c) images corrected without improvement, (d) image corrected with improvement in intensity.

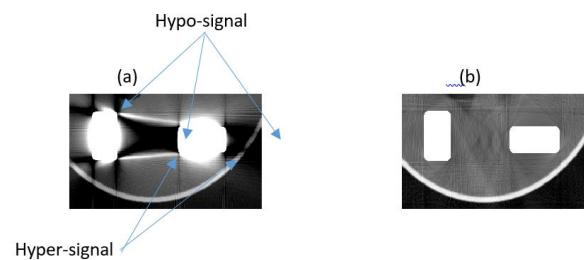


Figure 6. (a) Zoom of Figure 5 on the area of metal artifacts, (b) Results of the proposed algorithm.

In Figure 6a, we present a close-up view of the region affected by the presence of metal during the acquisition process of the tested object. This region experiences a phenomenon where the minimum and maximum absorptions of the two materials overlap, leading to a zone of uncertainty that results in the partial loss of the incident beam. Notably, this issue manifests as a hyper-signal, originating from the subband of lost energies (rays absorbed prematurely within the material), and a hypo-signal, arising due to the measured overcurrent in comparison to the theoretical intensity (visible as shadows in the image). Figure 6b illustrates the compelling results achieved by our proposed method in effectively mitigating both the hyper-signal and hypo-signal artifacts, thereby enhancing the overall image quality. Since there lacks a standardized quantitative approach for assessing CT MAR performance (Zhao et al., 2000), we have employed the peak signal-to-noise ratio (PSNR), a widely accepted criterion in the realm of image inpainting, to evaluate the algorithm's effectiveness.

$$PSNR = 10 \times \log_{10} \left(\frac{255^2}{\|Imag - Imag_0\|_2^2} \right) \quad (11)$$

Here, 'Imag' represents the image following inpainting, while 'Imag₀' denotes the original image.

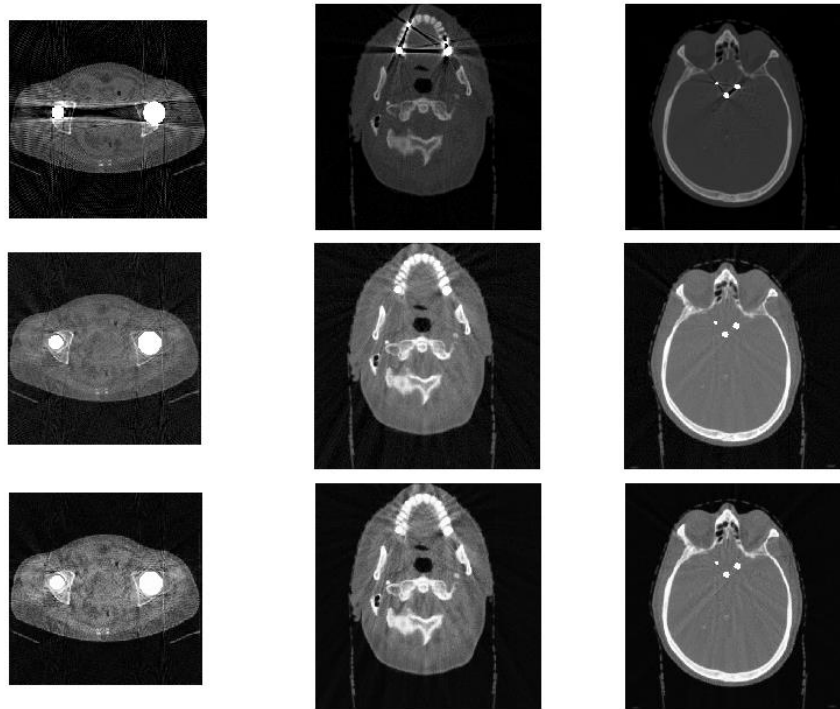


Figure 7. Numerical simulation results using the proposed correction method.

The first, second and third rows respectively show the images with artefacts, images corrected by the proposed method without enhancement and the images corrected with enhancement of their intensities. The first column is clinical CT image of pelvis with the two disk-shaped numerical metallic objects (titanium). Second column: jaw phantom with four disc-shaped metal objects. Third column: clinical CT images of the skull with three metallic objects.

The higher the PSNR value, the more favorable the performance. PSNR serves as a standard metric for quantifying the resemblance between an inpainted image and its genuine counterpart, rendering it a valuable benchmark. The PSNR_{in} value for the image in Figure 5b registers at 14.5. Upon applying the proposed correction method (Figure 5c), we observe an improvement, resulting in a PSNR_{out} of 18.26. Subsequent enhancement further elevates the PSNR to 20.04, as depicted in Figure 5d. Figure 7 illustrates the clinical computed tomography images. We do not know the original images, so it is not possible to calculate their PSNRs. The first, second and third row respectively show the images with artefacts, images corrected by the proposed method without enhancement and the images corrected with enhancement of their intensities. The proposed method makes it possible to successfully remove the streak artifacts without losing the morphological information, as shown in figure 6 (third row).

The outcomes of our study demonstrate the efficacy of the proposed algorithm in mitigating shadow and streak artifacts across various image types. The correction technique we've introduced successfully eradicates beam hardening artifacts without relying on sinogram data. Importantly, it operates independently of any prior knowledge regarding the energy spectra of the incident X-ray beam.

Conclusion

In this article, we have introduced a novel approach to mitigating metallic artifacts in CT images. Our proposed method encompasses four primary steps: image segmentation, gap filling within sinograms, image reconstruction, and enhancement of the reconstructed image. In the initial step, we employ a rapid algorithm based on K-means classification to extract metallic objects, thereby generating an image specifically highlighting metallic regions. The subsequent step involves the transformation of the metallic region image into the sinogram domain, allowing us to derive a trace of metallic elements within the sinogram. Through the identification of this trace, we effectively eliminate the corrupted projection caused by metallic objects from the original sinogram. To restore the values in the deleted regions, we apply a discrete cosine transform (DCT)-based method. Moving on to the third step, we reconstruct the image using the Filtered Back Projection (FBP)

technique while reintroducing the metallic objects into the image. Lastly, in the fourth step, we enhance the reconstructed image by equalizing contrast, thereby restoring the image intensities to their natural dynamic range. Our extensive numerical simulations and clinical applications have convincingly demonstrated the remarkable efficacy of our proposed method in significantly reducing metal artifacts and improving the overall image quality.

Scientific Ethics Declaration

The authors declare that the scientific ethical and legal responsibility of this article published in EPSTEM journal belongs to the authors.

Acknowledgements or Notes

* This article was presented as an poster presentation at the International Conference on Technology, Engineering and Science (www.icontes.net) held in Antalya/Turkey on November 16-19, 2023.

References

- Al-Ameen, Z., (2018). An improved contrast equalization technique for contrast enhancement in scanning electron microscopy images, *Wiley Periodicals, Inc. Microsc Res Tech.*1–11.
- Amorim, R.C., & Makarenkov, V., (2016). Applying subclustering and Lp distance in weighted K-means with distributed centroids, *Neurocomputing*, (173), 700–707.
- Arabi H. & Zaidi H., (2021). Deep learning-based metal artefact reduction in PET/CT imaging, *European Radiology*, <https://doi.org/10.1007/s00330-021-07709-z>.
- Bamberg, F., Dierks, A., Nikolaou, K., Reiser, M.F., Becker, C.R., Johnson T.R., (2011). Metal artefact reduction by dual energy computed tomography using monoenergetic extrapolation, *Eur Radiol*, 7, 1424-1429.
- Chang, Z., Ye, D. H., Srivastava, S., Thibault, J. B., Sauer K., & Bouman C. (2019). Prior-guided metal artifact reduction for iterative X-ray computed tomography, *IEEE Transactions on Medical Imaging*, 38(6).
- Frederique L., (2017). Identification et réduction de l'artefact métallique en tomographie à rayons X, *Thesis*, <https://tel.archives-ouvertes.fr/tel-01537663>.
- Garcia D., (2010). Robust smoothing of gridded data in one and higher dimensions with missing values", *Comput Stat Data Anal. 1*, 54(4), 1167–1178.
- King, J., Whittam, S., Smith, D., Al-Qaisieh, B., (2022). The impact of a metal artefact reduction algorithm on treatment planning for patients undergoing radiotherapy of the pelvi, *Physics and Imaging in Radiation Oncology*, (24), 138-143.
- Lin, C.-H., Chen, C. C., Lee, H. L., & Liao, J. R., (2014). Fast K-means algorithm based on a level histogram for image retrieval, *Expert Systems with Applications*, 41(7), 3276–3283.
- Mehranian, A., Ay, M.R., Rahmim, A., & Zaidi, H. (2013). X-ray CT metal artifact reduction using wavelet domain L0 sparse regularization, *IEEE Transactions on Medical Imaging*, 32(9), 1707–1722
- Müller, J., & Buzug, T. M., (2009) Spurious structures created by interpolation-based CT metal artifact reduction, *Medical Imaging 2009: Physics of Medical Imaging*, 72581Y.
- Park, H. S., Hwang, D., & Seo J. K., (2016). Metal artifact reduction for polychromatic X-ray CT based on a beam-hardening corrector, *IEEE Transactions on Medical Imaging*, 35(2).
- Tan, X., & Triggs, B., (2010), Enhanced local texture feature sets for face recognition under difficult lighting conditions, *IEEE Transactions on Image Processing*, 19(6), 1635–1650.
- Usman Ghani, M., & Clem Karl W., (2020). Fast enhanced CT metal artifact reduction using data domain deep learning. *IEEE Transactions on Computational Imaging*, (6).
- Wang, G., Garcia, D., Liu, Y., Richard de Jeu, C.D., Johannes Dolman, A., (2012). A three-dimensional gap filling method for large geophysical datasets: Application to global satellite soil moisture observations, *Environmental Modelling & Software*, 30, 139-142.
- Zhang, Y., & Yu, H., (2018). Convolutional neural network based metal artifact reduction (et al., 2022) in X-ray computed tomography. *IEEE Trans Med Imaging*, 37(6), 1370-1381.
- Zhang, Y., Pu, Y.F., Hu J.R., Liu, Y., & Zhou, J.-L., (2011). A new ct metal artifacts reduction algorithm based on fractional-order sinogram inpainting, *Journal of X-ray science and technology*, 19(3), 373–384.

Zhao, S., Robertson, D. D., Wang, G., Whiting, B., and Bae, K. T., (2000). X-ray CT metal artifact reduction using wavelets: an application for imaging total hip prostheses, *IEEE Transactions on Medical Imaging*, 19(12), 1238–1247.

Author Information

Abdessalem Benammar

Research Center in Industrial Technologies (CRTI),
P.O.Box 64, Cheraga 16014, Algiers, Algeria.
Contact e-mail: a.benammar@crti.dz

Aicha Allag

Research Center in Industrial Technologies (CRTI), P.O.Box
64, Cheraga 16014, Algiers, Algeria.

Imad Araar

Research Center in Industrial Technologies (CRTI),
P.O.Box 64, Cheraga 16014, Algiers, Algeria.

Ahmed Benyahia

Research Center in Industrial Technologies (CRTI), P.O.Box
64, Cheraga 16014, Algiers, Algeria.

Redouane Draï

Research Center in Industrial Technologies (CRTI),
P.O.Box 64, Cheraga 16014, Algiers, Algeria.

To cite this article:

Benammar, A., Allag, A., Araar, I., Benyahia, A. & Draï, R. (2023). Metal artifact reduction in CT images through sinogram data inpainting. *The Eurasia Proceedings of Science, Technology, Engineering & Mathematics (EPSTEM)*, 26, 770-779.